

Controlling photonic structures using optical forces

Gustavo S. Wiederhecker, Long Chen, Alexander Gondarenko, and Michal Lipson
School of Electrical and Computer Engineering, Cornell University, Ithaca, New York 14853, USA.

The downscaling of optical systems to the micro and nano-scale results in very compliant systems with nanogram-scale masses, which renders them susceptible to optical forces. Here we show a specially designed resonant structure for enabling efficient static control of the optical response with relatively weak optical forces. Using attractive gradient optical forces we demonstrate a static mechanical deformation of up to 12 nanometers in the resonator structure. This deformation is enough to shift the optical resonances by 6 optical linewidths.

INTRODUCTION

The use of optical forces to manipulate small particles is an important subject with applications ranging from manipulation of living cells by optical tweezers [1] to optical cooling in atomic physics [2]. More recently, the downscaling of optical systems to the micro and nano-scale resulted in very compliant systems with nanogram-scale masses, rendering them susceptible to optical forces [3, 4, 5, 6]. In fact, optical forces have been exploited to demonstrate chaotic quivering of microcavities [7], optical cooling of mechanical modes [8, 9, 10], actuation of a tapered-fiber waveguide [11], and excitation of the mechanical modes of silicon nano-beams [12]. The challenge in controllably manipulating the optical response of photonic structures using optical forces is that large optical forces are required, in order to induce appreciable changes in the structures geometries. Here we show a specially designed resonant structure for enabling efficient static control of the optical response with relatively weak optical forces. We demonstrate a static mechanical deformation of up to 12 nanometers in the geometry of a silicon nitride structure, using one milliwatt of optical power. Because of the optical response sensitivity to this deformation, such optically induced static displacement introduces resonance shifts spanning almost six resonance linewidths.

RESULTS

The photonic structure is composed of two coupled ring resonators with optical response sensitive to optical force-induced mechanical displacement. As shown in Fig. 1a, the structure is composed of a pair of vertically stacked silicon-nitride (SiN_x) rings held by very thin spokes and a pedestal [13]. The spokes are designed to reduce the mechanical stiffness of the cavity, increase the sensitivity to the optical forces between the rings, and at the same time induce only negligible scattering for light circulating near the outside edge of the rings. Due to the relatively small refractive index of SiN_x ($n \approx 2.0$), strong optical coupling can occur for relatively large gaps between the top and the bottom resonator ($g \approx 1 \mu\text{m}$). As a result

of this coupling, the transverse mode profile splits into symmetric (S, Fig. 1b) and antisymmetric (AS, Fig. 1c) combinations, leading to two distinct resonant frequencies. Figure 1d shows an example of the resonance wavelength splitting (centered at 1554.8 nm) for the transverse electric (TE) mode of a 30 μm diameter ring, obtained from numerical simulations. One can see that the splitting depends exponentially on the separation gap. Such steep gap dependence of the resonant frequencies on the separation translates into strong gradient optical forces between the rings [5, 6]. For symmetric and antisymmetric modes, the induced optical forces are attractive and repulsive, respectively.

We measured large splitting between the symmetric and antisymmetric optical modes in the fabricated structure, evidencing the predicted optical coupling between the cavities. Figure 2a we show the optical transmission for input light with transverse electric polarization for a 30 μm diameter rings (shown in Fig. 1a) with a coupling gap between the waveguide and the rings of 550 nm. The resonances are labelled with the azimuthal mode order m and transverse profile. They are identified by comparing their measured free spectral ranges with numerical simulations. The typical loaded optical quality factors for TE_m^+ and TE_m^- resonances were $Q = 8 \times 10^4$ (finesse $\mathcal{F} = 670$) and $Q = 2 \times 10^4$ ($\mathcal{F} = 150$), respectively.

We demonstrate experimentally the control of the photonic structure's response, i.e. the tuning of the resonance splitting with optical forces. As illustrated in the schematic of Fig. 2b, we use a pump laser to induce resonance shift and a weak probe laser to read-out the cavity response (see methods for details). As indicated in Fig. 2a, the control laser (blue arrow) is tuned to the minimum transmission point of a symmetric optical resonance ($TE_{m=76}^+$). We chose this resonance due to its higher finesse, resulting in higher intra-cavity energy and consequently stronger optical force. The probe laser wavelength is swept across the shaded region to read out the resonance shift ($\delta\lambda$) for both S and AS modes. The optical resonant wavelength shifts are plotted in Fig. 2c. One can see that one resonance is blue shifted ($TE_{m=75}^-$) while the other is red shifted ($TE_{m=75}^+$). The splitting between the two resonances induced by the optical forces shown in Fig. 2c confirms the theoretical prediction re-

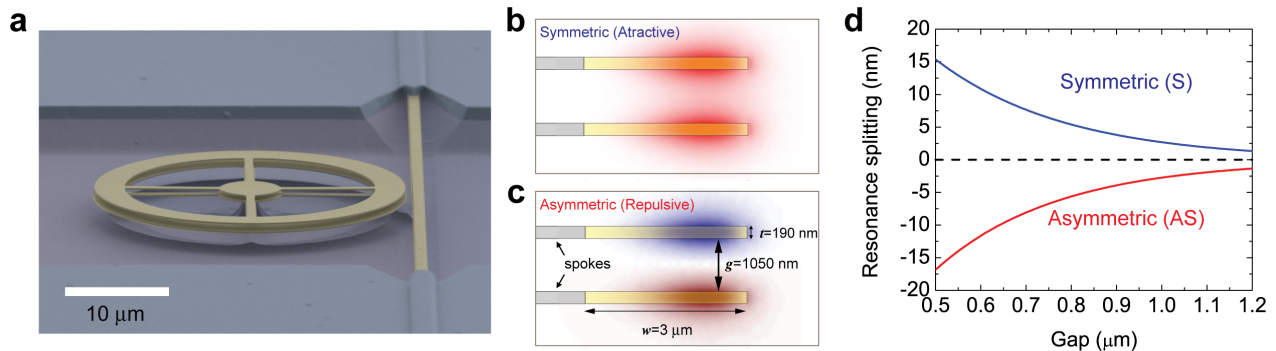


FIG. 1: **Design of a resonant cavity sensitive to optical gradient forces.** (a) Scanning electron micrograph of two vertically stacked ring cavities. (b,c) Cross-section of the ring region showing the simulated coupled electric field distribution for the symmetric (b) and antisymmetric (c) TE optical modes supported by the coupled cavities. The ring thickness is $t = 190$ nm, width $w = 3$ μm and inter-ring gap $g = 1$ μm . The symmetric mode leads to attractive forces, while the antisymmetric gives repulsive forces. (d) Typical simulated resonant wavelength splitting of the S and AS optical modes as the inter-ring gap distance is changed. At $g = 1$ μm the wavelength splitting spans about 5 nm.

ported by Rakich et al [6]. In particular, the control of the antisymmetric mode constitutes the first observation of static optical gradient force attraction between two resonant cavities. Note that the observed asymmetry of the splitting between the S and AS modes is due to thermo-optic effects present in the structure. This is because the wavelength shift induced by the optical force has opposite signs, positive for S and negative for the AS mode, while the shift induced by the thermo-optic effect has the same positive sign.

The thermal and the micromechanical contributions to the frequency splitting can be isolated. Considering the group index of the ring (extracted from the free spectral range), the thermo-optic coefficient of $\partial n/\partial T = 4 \times 10^{-5}$ for SiN_x and the optomechanical coupling parameter. The optomechanical coupling parameters for S and AS resonances are obtained from the numerical simulation of the cavity's optical response. For a 1 μm gap inter-cavity gap they have the numerical values $\kappa_{OM}^+ = -9.4 \times 10^{-3}$ and $\kappa_{OM}^- = 9.5 \times 10^{-3}$. The resonance splitting curves after removal of the thermal effect contribution are shown in Fig. 2d. The maximum optomechanical shift is calculated to be $\delta\lambda \approx 110$ pm, which spans as much as 6 resonance linewidths of the symmetric optical mode.

The maximum change in the gap between the two rings induced by the optical force is estimated from the splitting curves shown in Fig. 2d and the optomechanical coupling factors to be $\delta g = -12$ nm. The tuning of this gap with optical power coupled into the cavity is shown in Fig. 3. Using a spring constant of $k = 2.3$ N/m, calculated from numerical simulations of the cavity's mechanical response, the optical force on each ring can be estimated from the usual linear relation $F = k\delta g/2$. The left-side scale in Fig. 3 shows that a maximum force magnitude of 13.8 nN is achieved for 1 mW of coupled pump

power.

We verified that the impact of undesirable optically induced mechanical oscillations in our structure is minimal by measuring the dynamic optical response. We measured the temporal oscillation of the transmitted pump laser, and calculated the corresponding resonant wavelength oscillation caused by the mechanical oscillations. For the more sensitive symmetric resonance (higher Q), the resonance wavelength oscillation (with coupled pump power of 1 mW) is estimated to be 10 pm. This wavelength oscillation corresponds to only 9 % of the static wavelength shift shown in Fig. 2d (110 pm). These oscillations introduce some noise in the optical response. They could however be reduced by targeting lower mechanical quality factor cavities using, for instance, a pressurized environment or specific spokes design [13].

We show that significant optical force actuation is achievable by exploring interacting optical microcavities. The particular cavity design explored in this work provides high mechanical sensitivity to such forces. For instance, within the optical and mechanical quality factors explored here, the thermal effects and optomechanical oscillations are shown to be of secondary importance. This is an important step towards enabling recently proposed functionalities for optomechanical devices, such as self-aligning and optical corralling behaviour [6]. These advances on the static actuation of photonic microcavity structures using optical forces should enable future micro-optomechanical systems (MOMS) with novel and distinct functionalities.

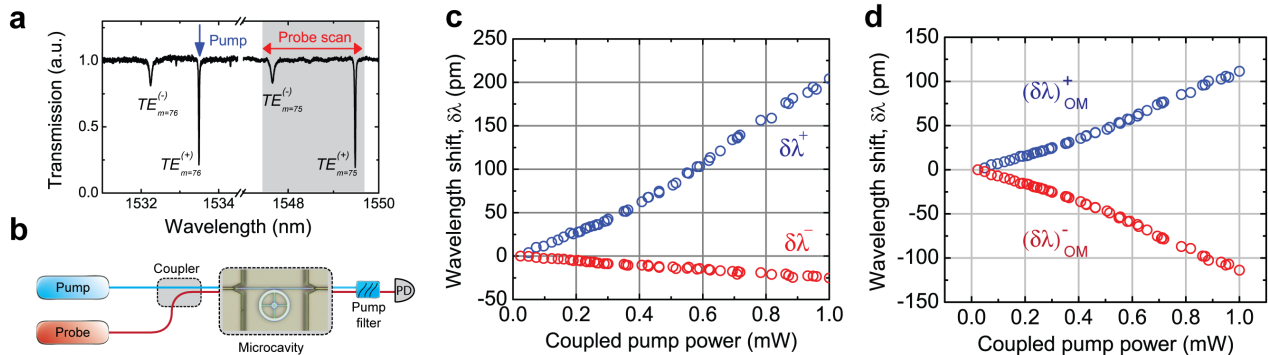


FIG. 2: **Demonstration of gradient force control of cavity resonances.** (a) Optical transmission of the fabricated device shown in Fig. 1a. The S (TE_m^+) and AS (TE_m^-) are highlighted. The pump (blue arrow) is coupled to the S ($m = 76$) mode while the probe scans over the AS/S ($m = 75$) resonance pair. (b) Schematic of the experimental setup. The pump and probe laser light are coupled and launched into the device, residual pump is filtered out and detected by the photodiode (PD). (c) Measured resonance splitting as a function of the pump power coupled to the cavity. The blue curve represents the S mode ($TE_{m=75}^+$) while the red curve represents the AS mode ($TE_{m=75}^-$). (d) Wavelength shift induced by the optical force ($\delta\lambda_{OM}$) without the thermal effect contribution

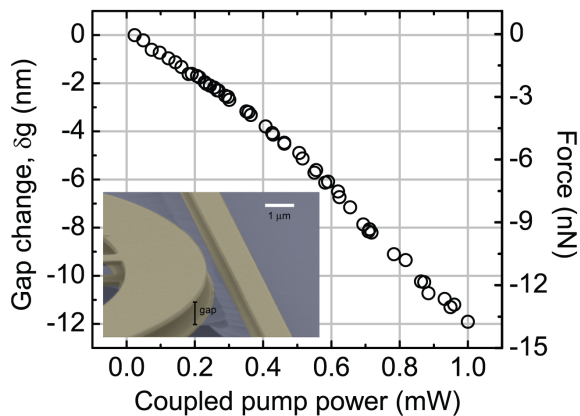


FIG. 3: **Inter-cavity gap change and optical force.** Change in the gap between the resonators (left scale) induced by the optical force (shown in the right scale). The inset shows a zoom of scanning electron microscope image of the cavity.

Methods

Device fabrication

The two layers (190 nm thick each) of stoichiometric SiN_x were deposited using low-pressure chemical vapour deposition (LPCVD) while the 350 nm thick SiO_2 layer was deposited by plasma-enhanced chemical vapour deposition (PECVD). The underlying substrate is a 5 μm SiO_2 formed by thermal oxidation of a silicon wafer. The two-stacked disks that form the resonator are patterned in a wheel shape and hold apart by a tiny silicon oxide (SiO_2) hub. The whole cavity structure is sitting on

top of SiO_2 pedestal as illustrated in Fig. 1a. Both the wheels and the coupling waveguides were patterned using a single step electron beam lithography followed by an anisotropic CHF_3/O_2 dry etch to define the structure. Because a single electron beam step is used, the coupling waveguides are formed as a double stack (see inset on 3). After depositing a 1 μm thick protective SiO_2 cladding using PECVD, we use optical lithography to pattern the spun photoresist with a rectangular window around the resonators. In order to release the structure, the device is immersed in buffered hydrofluoric acid for an isotropic etch of SiO_2 in the window region. To avoid stiction of the stacked disks, the device is subsequently dried using a critical point dryer. After the structure is released, the stress in the nitride films induces some bending of the rings in the vertical direction. This bending can be noticed in the SEM shown in Fig. 2a. Due to this bending, the actual gap between the resonators is estimated from the SEM image to be 1050 nm.

Experimental set-up

The set-up used to actuate and probe the cavity is illustrated in Fig. 2b. It consisted of two tuneable external cavity diode lasers combined using a 3 dB directional coupler. Due to the high insertion loss of our devices (≈ 16 dB), the pump laser was pre-amplified using an erbium doped fibre amplifier (not shown in the schematic of Fig. 2b). The laser light was coupled in and out of the chip using a pair of lensed optical fibres. The pump laser excited the optical resonance around 1533.5 nm and the probe laser wavelength was swept through a range spanning a pair of symmetric ($TE_{m=75}^+$) and antisymmetric ($TE_{m=75}^-$) resonances (see Fig. 2a). After col-

lecting the light from the output of the coupling waveguide, we used an interferometric filter (centre wavelength 1550 nm, bandwidth 10 nm) to reject any residual pump light. The probe laser light is then detected using either a Newport 818-IR low-power photodetector (when measuring the transmission spectrum) or a New Focus 1811 125 MHz bandwidth photodetector for the time-resolved measurements.

Coupled pump power calibration

The input pump power (P_{in}) launched in the coupling waveguides is estimated from the measured insertion loss of our devices (≈ 16 dB). As the pump power is increased however the cavity resonance is altered as well as the extinction ratio at the on-resonance transmission. The minimum cavity transmission is observed to change from at low input pump power ($P_{in} = 30 \mu\text{W}$) to at the highest power ($P_{in} = 2.2$ mW). We believe this reduction in the extinction ratio is caused by geometry-induced change in the cavity-waveguide optical coupling [11]. By taking into account the input power dependence of the on-resonance transmission, the relation between the pump power coupled to the cavity (coupled pump power) and the input pump power is corrected for each different input power. The on-resonance pump power coupled into the cavity (P_c) is given by $P_c = (1 - T_{on})P_{in}$, where is the input pump power into the coupling waveguide [11].

Time-domain measurements

The temporal response of the resonator was investigated by analyzing the time-domain response of the transmitted pump laser. Under the maximum power explored here (1 mW of coupled pump power) the measured relative oscillation amplitude in the pump transmission was $\delta P/P \approx 0.5$. By fitting a lorentzian line-shape to the pump resonance, one can map this power fluctuation into a drift of the resonance wavelength. For small pump detuning (< 5 pm) we have the maximum wavelength drift for a given power fluctuation. Under this condition the estimated wavelength drift is approximately 10 pm, which corresponds roughly to half pump resonance linewidth. Inspecting the RF spectrum of the transmitted pump laser we also identified the mechanical resonances responsible for the observed oscillations. For 1 mW of coupled pump power, the strongest RF resonances were observed at 6.15 MHz and 10.13 MHz. The mechanical quality factors for the measured resonances were $Q_M \approx 7$ and $Q_M \approx 15.8$, respectively.

Acknowledgements

This work was supported in part by the National Science Foundation under grant 00446571. The authors also acknowledge partial support by Cornell University's Center for Nanoscale Systems. This work was performed in part at the Cornell Nano-Scale Science & Technology Facility (a member of the National Nanofabrication Users Network) which is supported by National Science Foundation, its users, Cornell University and Industrial.

-
- [1] A. Ashkin and J. Dziedzic, *Science* **235**, 1517 (1987).
 - [2] T. Hansch and A. Schawlow, *Optics Communications* **13** (1975).
 - [3] M. Antonoyiannakis and J. Pendry, *Physical Review B* **60**, 2363 (1999).
 - [4] J. Ng, C. Chan, P. Sheng, and Z. Lin, *Optics Letters* **30**, 1956 (2005).
 - [5] M. Povinelli, M. Loncar, M. Ibanescu, E. Smythe, S. Johnson, F. Capasso, and J. Joannopoulos, *Optics Letters* **30**, 3042 (2005).
 - [6] P. Rakich, M. Solja, and E. Ippen, *Nature Photonics* **1**, 658 (2007).
 - [7] T. Carmon, M. C. Cross, and K. J. Vahala, *Physical Review Letters* **98**, 167203 (2007).
 - [8] T. Kippenberg and K. Vahala, *Optics Express* **15**, 17172 (2007).
 - [9] T. Kippenberg and K. Vahala, *Science* **321**, 1172 (2008).
 - [10] A. Schliesser, R. Rivière, G. Anetsberger, O. Arcizet, and T. Kippenberg, *Nature Physics* **4**, 415 (2008).
 - [11] M. Eichenfield, C. P. Michael, R. Perahia, and O. Painter, *Nature Photonics* **1**, 416 (2007).
 - [12] M. Li, W. Pernice, C. Xiong, T. Baehr-Jones, M. Hochberg, and H. Tang, *Nature* **456**, 480 (2008).
 - [13] G. Anetsberger, R. Rivi, A. Schliesser, O. Arcizet, and T. Kippenberg, *Nature Photonics* **2**, 627 (2008).